Appl. Phys. B 70, 903–910 (2000) / Digital Object Identifier (DOI) 10.1007/s003400000259

Applied Physics B
Lasers
and Optics

Comparison of laser-induced and planar laser-induced fluorescence measurements of nitric oxide in a high-pressure, swirl-stabilized, spray flame

C.S. Cooper*, **N.M. Laurendeau**

Flame Diagnostics Laboratory, School of Mechanical Engineering, 1288 Mechanical Engineering, Purdue University, West Lafayette, IN 47907-1288, USA (Fax: +1-765/494-0539, E-mail: ccooper@ecn.purdue.edu)

Received: 23 November 1999/Revised version: 17 January 2000/Published online: 27 April 2000 –

Abstract. We report spatially resolved linear laser-induced fluorescence (LIF) and planar laser-induced fluorescence (PLIF) measurements of nitric oxide (NO) in a pre-heated, high-pressure (4.27 atm), lean direct-injection (LDI) spray flame. The feasibility of using PLIF in lieu of LIF is assessed with respect to measuring NO concentrations in high-pressure LDI spray flames. NO is excited via the resonant $Q_2(26.5)$ transition of the $\gamma(0, 0)$ band while a non-resonant wavelength is employed to subtract background interferences. LIF detection is performed in a 2-nm region centered on the $\gamma(0, 1)$ band. PLIF detection is performed in a 68-nm window that captures fluorescence from several vibrational bands. An in situ NO doping scheme for fluorescence calibration is successfully employed to quantify the LIF signals. However, a similar calibration scheme for the reduction of PLIF images to quantitative field measurements is plagued by the laser-excited background. Excitation scans and calibration comparisons have been performed to assess the background contribution for PLIF detection. Quantitative radial NO profiles measured by LIF are presented and analyzed so as to correct the PLIF measurements to within the accuracy bars of the LIF measurements via a single-point scaling of the PLIF image.

PACS: 32.50.+d; 47.70.Fw

This investigation is concerned with the development of a quantitative, non-intrusive, scheme by which NO concentrations can be measured in high-pressure spray flames. Several researchers have utilized optical measurements of minor species in such flames. Allen et al. [1] obtained qualitative [OH] images in heptane–air spray flames formed via both solid and hollow-cone nozzles and burned at pressures of 0.1–0.8 MPa. Excitation of OH was achieved by employing the $P_1(8)$ transition at 285.67 nm. The effect of interfering PAH fluorescence was assessed by using a spectrometer to separate the fluorescence spectrum into individual features. A laser-induced signal exhibiting features at 350 nm, 400 nm, and 450 nm was found on a quasi-continuum background at lower pressures. The strength and spectral characteristics of this broad background were observed to be independent of excitation wavelength within a 5-nm region centered on the $P_1(8)$ transition, which indicated the presence of a broad absorbing species such as a large molecular weight hydrocarbon. As the pressure rose, the above spectral features became non-discernable and exhibited a P^2 increase in fluorescence strength.

In an extension of this work, Allen et al. [2] performed similar [OH] imaging in ethanol flames and further assessed the effects of PAH interferences. While alluding to potential NO measurements, Allen et al. [2] suggested that excitation near 226 nm may produce more severe laser attenuation and hence PAH fluorescence. To test this conjecture, Upshulte et al. [3] obtained qualitative PLIF images of NO, O_2, and fuel vapor by employing excitation wavelengths of 226 nm and 308 nm. Measurements were made for ethanol fuel in the same high-pressure, spray-flame combustor used by Allen et al. [2]. As expected, a broad interference signal attributed to PAHs was discovered and assigned to a nominal 5% of the NO signal at atmospheric pressure.

Locke et al. [4] utilized PLIF to image hydroxyl concentrations in a high-pressure (10–14 atm) combustor supplied with Jet-A fuel (0.59–0.83 kg/s) through lean direct-injection ($\phi = 0.41 - 0.53$) with preheated air (811–866 K). Though this work only assessed the qualitative distribution of OH radicals in the reacting flow, the combustor was designed to simulate actual gas turbine conditions. The authors found that elastically scattered light and PAH fluorescence were not evident in the downstream regions of their LDI-based combustor. This was a significant finding, as quantitative LIF measurements in harsh environments are an end-goal of optical diagnostics in spray flames.

Cooper and Laurendeau [5] developed a saturated-LIF (LSF) technique capable of quantitative measurements of NO concentration in an atmospheric, unconfined, swirl-stabilized spray flame based on a lean direct-injection design. The burner incorporated a helical swirler with a central hollow-cone, pressure-atomized spray nozzle supplied with liquid heptane. A converging/diverging orifice was positioned im-

*Corresponding author.

mediately after the swirler/injector assembly. The diagnostic technique incorporated a subtraction method to remove Mie-scattering background from the NO fluorescence signal. Because of the inherently low sensitivity of LSF to variations in the electronic quenching rate coefficient, a fluorescence calibration developed in a reference flame could be successfully transported to the LDI spray flame.

Cooper et al. [6] continued the previous work by comparing linear-LIF-based techniques, both point-LIF and planar-LIF, to the LSF method. Because the linear techniques could not employ a transported calibration, the entire flow field was scaled by the ratio of a linear to a saturated fluorescence signal at a single point in the measurement field. This procedure produced an NO field that fell entirely within the accuracy bars of the more quantitative LSF measurements. In this way, Cooper et al. [6] demonstrated the feasibility of a potential calibration method for high-pressure LIF measurements of NO in spray flames.

In a similar manner, Ravikrishna et al. [7] quantified PLIF images of NO in partially-premixed ethane flames by scaling the entire image based on a single LSF point measurement. The authors chose the partially premixed flame as a robust test case which included large gradients in temperature, species concentrations, and the electronic quenching rate coefficient. Despite using a single-point scaling method, over 90% of the PLIF measurements fell within the accuracy bars of the LSF data.

The current investigation represents the fourth contribution to a comprehensive high-pressure project aimed at understanding NO_x emissions from an LDI burner. The end-goal of this program is characterization of NO profiles and emissions at 1–10 atm, with parametric studies of air preheat, swirl, and overall equivalence ratio. In this fourth paper, we assess the utility of planar laser-induced fluorescence for quantitative measurements of NO in the harsh environment of a high-pressure spray flame. In particular, broad-band PLIF measurements are compared to narrow-band LIF measurements to evaluate the extent to which PLIF can be made quantitative despite strong interferences from hot O_2 and hydrocarbon intermediates (PAHs).

1 Experimental apparatus

1.1 Optical system

Following the methods described by Reisel et al. [8], excitation of NO is achieved via the $Q_2(26.5)$ line of its $\gamma(0, 0)$ band at ≈ 225.58 nm. The fundamental (1064 nm) from a Spectra-Physics GCR-3 Nd:YAG laser is frequency doubled (532 nm) and used to pump a tunable PDL dye laser. Rhodamine 610 and Rhodamine 590 dyes are employed to generate the PDL fundamental at 572.54 nm. A WEX wavelength extender is used to frequency-double the dye laser output to 286.27 nm, followed by frequency mixing with the Nd:YAG fundamental to produce the required ≈ 225.58 nm laser beam. The system is equipped with a Fabry–Pérot wavelength stabilization system to control PDL drift [9]. The maximum energy obtained for the mixed beam is ≈ 2.5 mJ/pulse. This energy is reduced by a factor of ten with neutral density filters so as to operate in the linear regime of NO excitation. The fluorescence from the probe volume (800 μm in diameter by 1 mm long) is monitored via a 1/2-m monochromator with a Hamamatsu R106UH-HA PMT specially wired for high temporal resolution [10]. In addition, two CVI LWP-0-R226-T235-237-PW-2037-UV long-wave pass, dichroic beamsplitters designed to reject 226-nm radiation and to transmit wavelengths greater than 233 nm at zero angle of incidence are used to improve the signal-to-background ratio of all measurements within the spray sheath [11]. The manufacturer's spectral traces for these mirrors indicate a transmission of $\approx 2\%$ at 226 nm and $\approx 80\%$ at 236 nm. The NO fluorescence signal is averaged over 600 laser shots, whereas the off-line background is averaged over 300 shots.

The same excitation transition employed for the LIF measurements of NO is used for the PLIF measurements, namely the $Q_2(26.5)$ line within the $\gamma(0, 0)$ band at ≈ 225.58 nm. The generated sheet of laser irradiance is ≈ 850 μm wide. A Princeton Instruments model ICCD-576TC-RG proximity-focused ICCD detector incorporating a 578×384 pixel, charge-coupled device (CCD) with 23-μm-square pixels was utilized for detection of the NO fluorescence. The fluorescence was focused on the ICCD detector by utilizing an aberration-corrected, five fused-silica element, 105-mm-focal-length $f/4.5$ lens, such that each pixel corresponds to a ≈ 67 μm square in the image plane of the flame. The filter set consisted of a wide-band interference filter (98-nm FWHM) spectrally centered at 250 nm coupled with three CVI LWP-0-R226-T235-237-PW-2037-UV mirrors. This scheme collects fluorescence from several vibrational bands (68-nm FWHM), as opposed to the restricted (0,1) band used in the LIF measurements [12].

An ICCD thermoelectric cooler was used in conjunction with an external water chiller/circulator to reduce the temperature of the CCD to $-34\,^{\circ}$C. A pulse generator (Princeton Instruments model FG-100) was used to produce a gate of 20 ns to the ICCD. The NO fluorescence images were averaged over 1200 laser shots in order to achieve a sufficient signal-to-background ratio. Operation of the ICCD and supporting hardware was controlled by a detector controller (Princeton Instruments model ST-130). The user interface to the ICCD system was provided by Princeton Instruments WinSPEC software, which was also used for all image analysis and reduction.

1.2 High-pressure facility

The high-pressure vessel (see Fig. 1) is custom-built by Parr Instrument Co. (Peoria, IL) and incorporates a water jacket and three UV fused-silica windows for transmission of the beam and ensuing fluorescence. The vessel is rated at 3.1 MPa internal pressure and 700 K internal wall temperature. The stainless steel LDI module internal to the vessel (11.43 mm internal diameter) accommodates a fuel tube (3.175 mm diameter) that enters the module outside of the vessel. A 60° helical swirler (11.43 mm diameter) is mounted at the top of the fuel delivery tube. The swirler itself is tapped to allow a macrolaminate Parker-Hannifan hollow-cone, pressure-atomized spray nozzle (OD = 5.3 mm) to be directly threaded into the swirler. The nozzle is positioned vertically relative to a converging/diverging orifice (10.16 mm diameter at 40°). The depth of the nozzle below this orifice (5.64 mm) is adjustable via copper washers located at the bottom of the module. The orifice is mounted

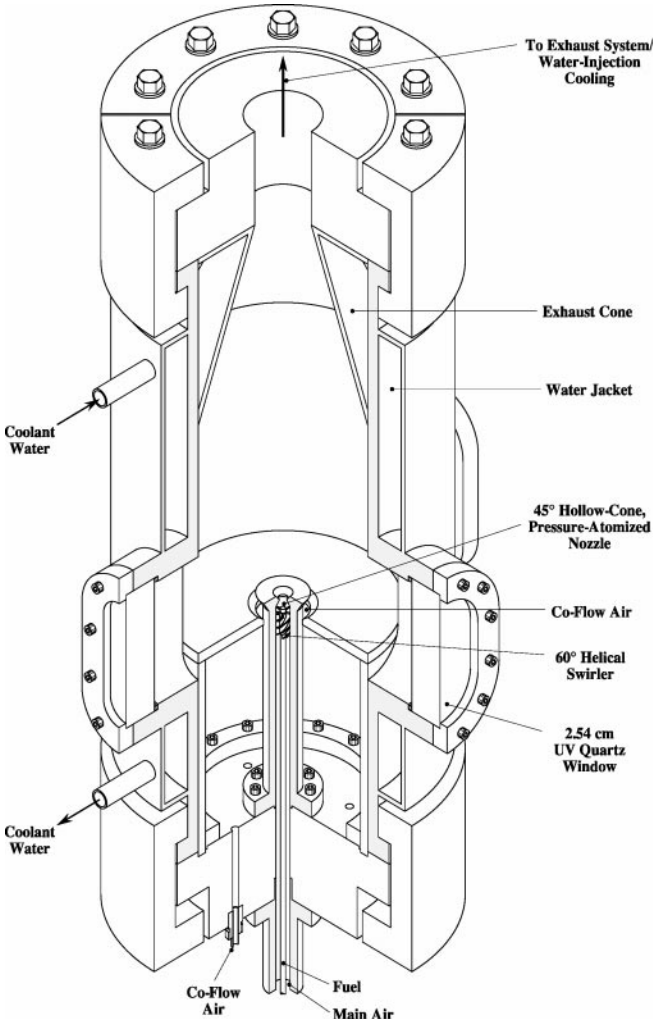

Fig. 1. Cutaway drawing of LDI burner and high-pressure vessel. The burner is constructed of stainless steel with a fuel tube entering co-axially at the bottom of the vessel. Air is directed through a five-vane, helical swirler (60°). Fuel is injected immediately after the swirler by utilizing a small pressure-atomized nozzle

to the stem via a threaded channel and can be adjusted further relative to the nozzle if needed. The main air is preheated in each experiment and delivered axially to the module axis. The co-flow air is introduced to the burner via three holes in the bottom flange. A cap assembly is fitted over the main stem which allows the co-flow air to enter the flowfield via the central orifice shown in Fig. 1. The purpose of the co-flow air is to aid in flame stabilization since the outer recirculation zone of the flame hinders flame stability.

The fuel delivery system incorporates a four-gallon, stainless-steel pressure vessel rated at 5.3 MPa. The stored heptane is pressurized with nitrogen at 1.5 MPa and metered via a rotameter flow controller. The air is provided from a building compressor. The air flows for the main and co-flow passages are adjusted with metering valves and monitored with Hastings fast-response thermal mass flow meters (model HFM-230). Preheating is achieved with two in-line air heaters controlled with voltage regulators. The maximum preheat air temperature is limited by boiling within the fuel tube, which leads to vapor lock in the injector.

The small size of the vessel (22.2 cm OD, 15.2 cm ID) requires a translation system capable of translating the full weight of the vessel both vertically and horizontally. The vertical translation stage (Daedal model 406014ET-MS-D2-L2-C4-M3-W1) is a modified single-axis series 406000ET linear table. The table has a travel of 101.6 mm, a positional accuracy of 89 μm, and a positional repeatability of ±51 μm. The horizontal stage (Daedal standard model 315801AT-ES-D4-L2-C2-M1-E1) is an open-frame linear table with a travel of 200 mm, a positional accuracy of 40 μm, and a positional repeatability of ±25 μm. Precise step control was achieved through an interface with LabVIEW software. The high-pressure vessel is mounted on the open-frame linear table via a base plate designed to secure the vessel and to permit feeding of air and fuel lines through the optical table.

1.3 Operating conditions

The LDI burner is operated at a pressure of 4.27 atm and a primary equivalence ratio $\phi_p = 0.9$ using liquid heptane metered at 0.36 g/s and air at 6.07 g/s. The air is preheated to 375 K to assist in vaporization and mixing of the fuel. Because of the intense mixing, the flames are essentially non-sooting and blue. An additional co-flow is introduced to aid in flame stabilization that reduces the overall equivalence ratio to 0.85, assuming complete entrainment into the combustion zone. A photograph of the flame is shown in Fig. 2. Note the non-sooting appearance and the symmetric structure of the flame.

2 Laser-induced fluorescence measurements

Our previous work addressed an excitation/detection scheme for use in atmospheric-pressure LDI flames [5]. In particular, excitation of the $Q_2(26.5)$ line of the $\gamma(0,0)$ band of NO at 225.58 nm is followed by detection of the $\gamma(0,1)$ band with a 2-nm window centered at 235.78 nm. An off-line wavelength at ≈ 225.53 nm is excited and monitored to determine any background for the NO fluorescence signal. This combination has been selected based on extensive

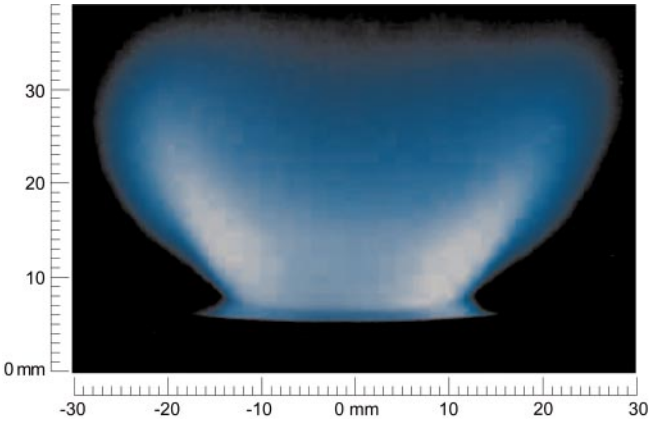

Fig. 2. Photograph of LDI flame at 4.27 atm ($\dot{m}_{fuel} = 0.36$ g/s, $\phi_p = 0.9$, $T_{air\ preheat} = 375$ K)

interference and background investigations [8, 12] and has shown considerable success in a variety of flames fueled with both gaseous and liquid fuels [8, 11, 13]. The scheme has been particularly useful in high-pressure (1–15 atm) $CH_4/O_2/N_2$ flames [13]. At atmospheric pressure, the utility of this approach lies in subtraction of Mie-scattering interferences that break through the monochromator despite the $\approx$ 10-nm separation between the excitation and detection wavelengths. At higher pressures, this scheme is critical to the detection of NO levels below 10 ppm owing to the background produced by the O_2 Schumann–Runge spectrum.

Previous work [14, 15] details linear LIF measurements for the LDI burner at pressures up to 5.35 atm. In particular, a calibration scheme was developed which allows in situ doping of NO through the spray flame with no apparent destruction. The calibration slope measurements in the spray flame were validated through comparisons with similar measurements in flames of known spectral and chemical characteristics [13].

2.1 Mie-scattering profiles

The influence of Mie scattering at 4 atm was assessed by measuring scattering profiles so as to locate regions of heavy droplet interference. Scattered light at the incident laser wavelength is passed through neutral density filters and collected via a 1/2-m monochromator in a 2-nm window centered at $\approx$ 226 nm. Figure 3 depicts the resulting Mie-scattering profiles, plotted as arbitrary units and presented only to visualize the spray structure. These profiles compare favorably with the expected profiles based on our 1-atm study, namely axisymmetric double-peaked profiles that reveal the spray sheath typically associated with strongly swirling spray flames [16].

2.2 LIF measurement scheme

Typical LIF measurements in harsh environments employ a calibration based on a well-characterized flame [5, 6]. The accurate transfer of a calibration from one flame environment to another requires that

$$[\mathrm{NO}]_{\mathrm{LDI,absolute}} = \left(\frac{Q_{\mathrm{e,\ LDI}}}{Q_{\mathrm{e,\ ref}}}\right)[\mathrm{NO}]_{\mathrm{LDI,relative}}; \quad (1)$$

in other words, the concentration measurements relative to the calibration obtained in the reference flame, $[\mathrm{NO}]_{\mathrm{LDI,relative}}$, must be scaled by the ratio of the electronic quenching rate coefficients in the LDI and reference flames. This procedure yields absolute concentration measurements, $[\mathrm{NO}]_{\mathrm{LDI,absolute}}$. Whereas species profiles for a flat, premixed reference flame can be accurately predicted via PREMIX [17], the LDI flame cannot be adequately modeled so as to provide the distribution of major species concentrations. Consequently, an estimate cannot be determined for the required ratio of local electronic quenching rate coefficients, and thus an in situ calibration method is required for LDI spray flames [14, 15].

The results from our atmospheric study demonstrate that the central region of the recirculation zone can provide a successful fluorescence calibration, barring any destruction of NO as it is transported from the reactants to this region [6]. Doped NO in spray flames must be transported through the rich regions surrounding the liquid droplets, possibly promoting NO destruction. Moreover, the degree of local partial premixing and the local strain rate could play a large role in the destruction of NO. These issues are not readily modeled for the LDI flame, so that an experimental validation is required for any in situ doping process. We have experimentally validated an in situ doping method for the LDI burner, whereby the flame was seeded with varying levels of NO and the fluorescence signals at these levels were measured. The measurement location was chosen to be the centerline location at a 35-mm axial height so as to reduce background interferences. NO was seeded into the flow through 3000-ppm doped nitrogen. After this experiment, the high-pressure vessel was immediately modified to incorporate a flat-flame McKenna burner and placed back into the translation assembly. Calibration measurements were then performed in the post-flame region of a lean ($\phi = 0.8$, 3.76 dilution ratio) $CH_4/O_2/N_2/NO$ flame at the same pressure. This flame is well characterized and has been utilized previously for spectral and calibration comparisons [13]. The excellent similarity of the calibration slopes demonstrated that NO destruction is not a significant factor in the transport of doped NO to the central region of LDI flames at pressures up to 5 atm [14, 15].

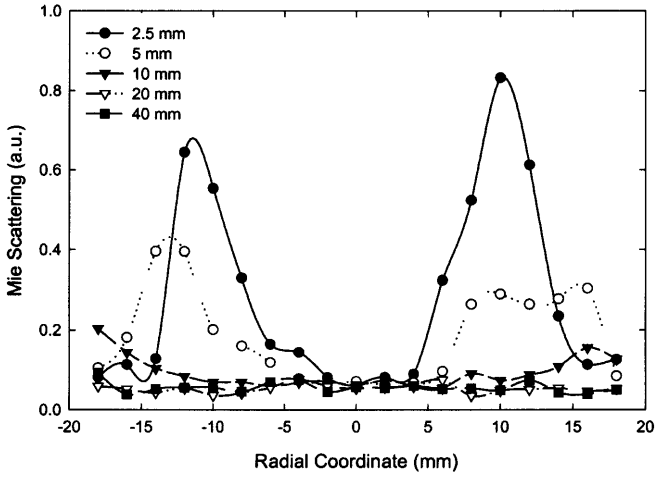

Fig. 3. Mie-scattering radial profiles for LDI flame at 4.27 atm ($\dot{m}_{\mathrm{fuel}} = 0.36$ g/s, $\phi_{\mathrm{p}} = 0.9$, $T_{\mathrm{air\ preheat}} = 375$ K)

2.3 LIF experimental method

To obtain NO profiles in the LDI spray flame, we employed the following experimental protocol. The quartz windows were cleaned at the start of the experiment to ensure minimal transmission losses owing to soot deposition. Soot deposition occurred only during flame ignition when the flame was burned rich while the vessel was sealed and brought to the operating pressure. The LDI flame was stabilized in the pressure vessel for a period of one to two hours to allow the vessel to reach a steady temperature. During this period, the wavelength-feedback system was initialized, which required an excitation scan over the $Q_2(26.5)$ transition. NO was then doped into the flame to obtain a NO

fluorescence calibration at the 35-mm centerline height specific to the experimental measurements. The translation system was then employed to translate the entire high-pressure vessel relative to the probe volume. In this manner, fluorescence profiles along the major diameter were mapped utilizing both on-line and off-line excitation wavelengths at each point, thus accounting for variations in O_2 fluorescence and Mie-scattering background throughout the flame.

Photodiodes placed at the optical entrance and exit of the vessel were utilized to measure laser-beam power ratios across the LDI flame and thus to calculate a global transmission (τ_{global}) at each axial height. This measurement represents beam extinction through the full diameter of the flame. The data reduction accounted for global extinction at each axial height by assuming equivalent extinction coefficients for both 226-nm and 236-nm radiation. The calculated τ_{global} was thus used to account for both beam extinction prior to reaching the probe volume and fluorescence trapping normal to the excitation beam. Power ratios were also measured through the entrance window to account for slight variations in the amount of soot deposition, which could affect the transmission of the excitation beam. The effect of soot deposition was thus calculated as a soot transmission (τ_{soot}) at each axial height. Recognizing that the flame is symmetric and that the photodiode used to measure the laser beam power is positioned prior to the vessel entrance window, the NO levels can be calculated via [14],

$$[\text{NO}]_{\text{ppm,rel}} = \frac{\text{LIF}_{\text{on},h} - \text{LIF}_{\text{off},h}}{m_{\text{net,cal}}} \cdot \frac{\tau_{\text{global,cal}} \times \tau_{\text{soot,cal}}}{\tau_{\text{global},h} \times \tau_{\text{soot},h}}. \qquad (2)$$

The LIF measurements designated $\text{LIF}_{\text{on},h}$ and $\text{LIF}_{\text{off},h}$ at a given height h above the burner are reduced to relative ppm values, $[\text{NO}]_{\text{ppm,rel}}$, by employing the 35-mm fluorescence calibration slope, $m_{\text{net,cal}}$. The term *relative* implies that the NO values are calculated relative to the fluorescence calibration at the temperature and electronic quenching rate coefficient corresponding to the 35-mm axial height location. Ratios of transmission values at the calibration height to those at the measurement height are necessary to correct the data, since the calibration slope $m_{\text{net,cal}}$ inherently includes the effects of losses at the calibration height. The resulting NO concentrations are thus expressed relative to the calibration point, to within any gradients in the temperature and electronic quenching rate coefficient throughout the measured region.

On a separate day, the calibration slopes were also measured at the centerline of each axial height. These calibration slopes require correction for extinction and soot transmission losses in a manner similar to the relative NO measurements. A final data reduction accounted for the ratio of the fluorescence calibration at a particular axial height to that at the 35-mm location, i.e.,

$$[\text{NO}]_{\text{ppm,abs}} = [\text{NO}]_{\text{ppm,rel}} \times \frac{m_{\text{net,cal}}}{\tau_{\text{global,cal}} \times \tau_{\text{soot,cal}}} \times \frac{\tau_{\text{global},h} \times \tau_{\text{soot},h}}{m_{\text{net},h}}. \qquad (3)$$

In this manner, each radial profile was analyzed via a calibration specific to that axial height, thus providing a measure of the absolute NO ppm level, $[\text{NO}]_{\text{ppm,abs}}$. Notice that the effect of global transmission and soot losses is now removed at a given axial height. Though these transmission values ultimately cancel in the final data reduction of (2) and (3), experimental accuracy requires that these quantities be measured during each separate experiment owing to a potential lack of repeatability in the data.

2.4 NO LIF profiles

Figure 4 demonstrates the corrected data whereby each radial profile is calibrated by the centerline fluorescence calibration at the particular axial height and plotted as a function of the radial coordinate. Accuracy bars are typically ±25% at the 95% confidence interval, with an average repeatability of 12%. In general, the NO profile at each axial height demonstrates a uniformity of the NO mole fraction throughout the central region of the LDI flame. In particular, note that the centerline value at each axial height is constant to within 15%. This can be attributed to the well-mixed nature of the internal recirculation zone for this geometry, as demonstrated by previous researchers [18, 19]. In particular, Terasaki and Hayashi [19] demonstrated fairly uniform radial temperatures within the recirculation zone in a similar

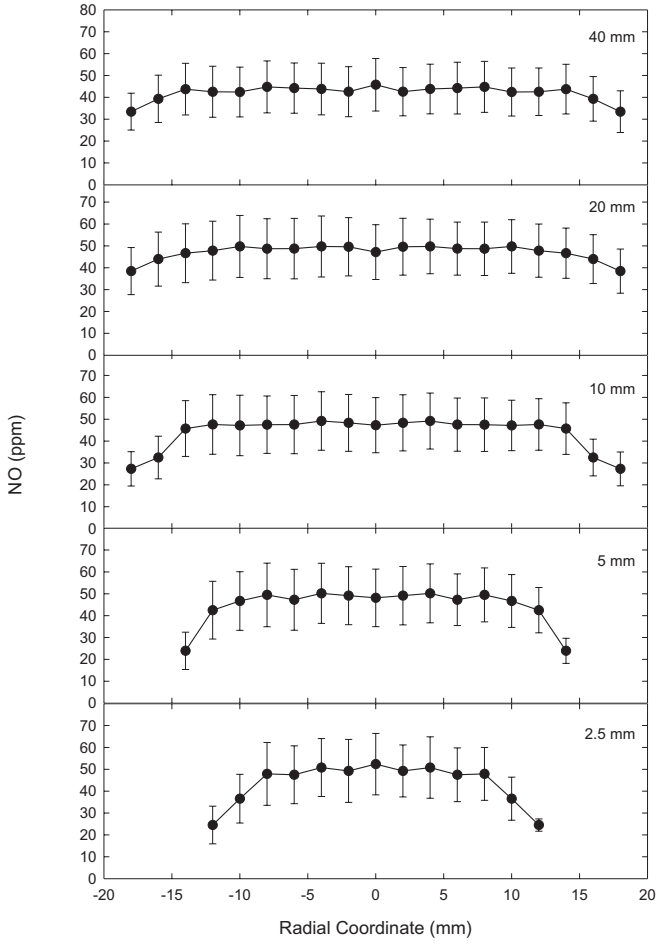

Fig. 4. Absolute NO (ppm) measurements in 4.27-atm LDI flame ($\dot{m}_{\text{fuel}} = 0.36$ g/s, $\phi_{\text{p}} = 0.9$, $T_{\text{air preheat}} = 375$ K). Radial NO profiles have been corrected for extinction and calibrated at each axial height

swirl burner. Our measurements are focused on this homogeneously mixed recirculation zone and therefore are limited by radial temperature gradients near the shear layer. Careful examination of Figs. 3 and 4 demonstrates that our measurements are spatially located between the centerline and the spray sheath, thus avoiding radial temperature gradients.

Since each radial profile is referenced to the calibration taken at its centerline, the profiles ultimately become skewed as the laser transmission decreases with increasing path length. Hence, those measurements taken past the centerline are preferentially lower, whereas those taken prior to the centerline are preferentially higher. It should be emphasized, however, that the centerline measurement for each axial calibration is an absolute measurement, as all effects other than possible NO destruction are inherently included in the calibration. To correct for the skewness of the NO profiles that resulted from absorption losses, the profiles were mirrored and averaged. A simple model was constructed to validate this correction technique for a range of absorption coefficient profiles and NO concentration profiles in an axisymmetric flow, recognizing that both the laser beam and NO fluorescence pass through different path lengths as a function of measurement position. The results indicate that this correction procedure is quite satisfactory owing to the centerline pivot point that the profiles are referenced to via the fluorescence calibration. The accuracy of the method obviously increases as the NO concentration profiles and the extinction coefficient become more uniform across the flame.

3 PLIF measurements

We have shown that the narrowband LIF technique yields excellent results despite the harsh environment of the spray flame [14, 15]. This fact permits us to consider PLIF as an additional tool by which to explore the NO concentration field. If the detected fluorescence is not plagued by Mie scattering or laser-induced interferences, i.e., O_2, PAH, or UHC fluorescence, then the opportunity exists to make quantitative images of NO concentration. In particular, the subtraction technique must employ two excitation wavelengths having common backgrounds within the broadband spectral window for PLIF.

3.1 PLIF excitation scan comparison

The narrowband detection window for LIF was chosen based on a common and small background at the two excitation wavelengths [13]. For the broadband detection window used in PLIF, off-line wavelength excitation should accurately mimic the Mie background; however, an accurate representation of any O_2 interferences cannot be guaranteed without further work. To experimentally assess the background in the PLIF detection window, an excitation image sequence was performed whereby the cumulative fluorescence from 1200 laser shots was summed on chip and normalized by the laser power. The laser excitation wavelength was shifted after each image so as to scan the spectral region of interest, namely 225.5 to 225.6 nm, thus encompassing the $Q_2(26.5)$ transition of NO. A 1 mm × 1 mm region in each image at the centerline of the 15-mm axial height was averaged and compared with a similar scan at the same location when utilizing narrowband LIF. The results of this comparison are shown in Fig. 5, where the scans have been normalized to a maximum signal level of unity. The on-line excitation wavelength is labeled at the $Q_2(26.5)$ transition, whereas the off-line excitation wavelength used in the LIF measurements is labeled near 225.52 nm. The off-line wavelength demonstrates an increased PLIF signal level relative to that for LIF. Since the LIF spectrum has been well characterized [13–15], we surmise that the off-line excitation wavelength likely excites an interference within the broadband detection window for PLIF that is not common to the on-line excitation wavelength.

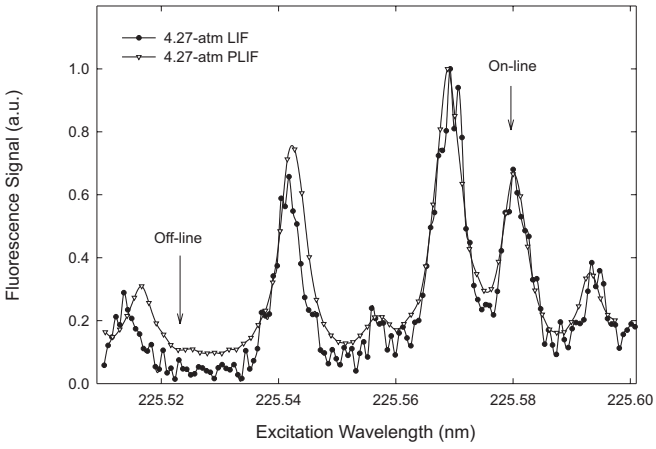

Fig. 5. Excitation scans in 4.27-atm LDI flame at $h = 15$ mm, $r = 0$ mm doped with ≈ 80 ppm NO using narrowband LIF detection and broadband PLIF detection. The NO on-line $Q_2(26.5)$ and the off-line excitation wavelengths are labeled

3.2 Calibration slope comparison

To better characterize the increase in background when using a broadband detection window, calibration measurements were performed whereby NO was doped into the flame in a manner identical to that for previous LIF measurements [14, 15]. The NO doping gas contained 3000 ppm NO in N_2 which was metered to achieve levels of less than 100 ppm in the flame products. A 1 mm × 1 mm square along the centerline in the well-mixed region was averaged and utilized to obtain a broadband calibration slope from the various doping levels. This region displays uniform narrowband calibration slopes which are independent of axial height owing to a lack of thermal gradients in the axial direction [15]. Hence, similar calibration slopes measured with narrowband LIF were taken at the same position in the flame for comparison. The two data sets, LIF and PLIF, were then normalized to unity at the maximum doping condition for on-line excitation. A comparison of the two calibration sets utilizing both on-line and off-line excitation is shown in Fig. 6. Whereas the on-line calibration slopes are very similar, the off-line calibration intercepts are quite different. The obvious shift validates the increased background observed in Fig. 5. To further emphasize the preferential off-line excitation, the ratio of

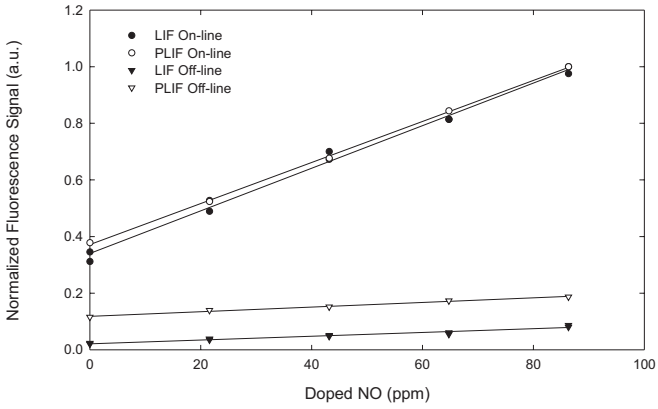

Fig. 6. NO fluorescence calibrations taken in 4.27-atm LDI flame using narrowband LIF detection and broadband PLIF detection. Both calibration curves have been normalized to unity at the maximum on-line doping condition. Note the background shift for off-line PLIF excitation

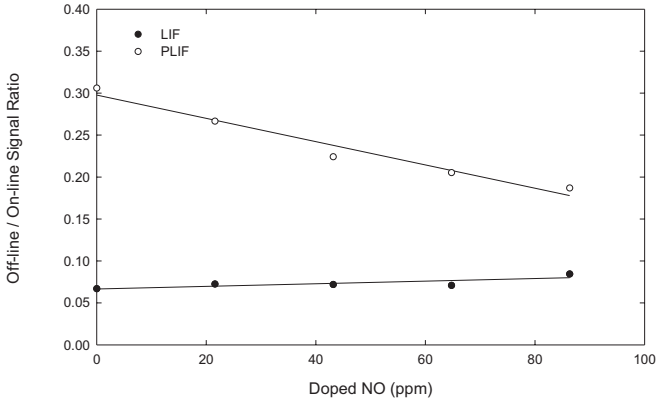

Fig. 7. Ratio of off-line to on-line calibration signal in 4.27-atm LDI flame for narrowband LIF detection and broadband PLIF detection. The LIF data demonstrate a ratio which is constant with doping level. The PLIF data demonstrate a decrease with increasing NO concentration, revealing a preferential excitement of interfering species by the off-line wavelength within the broadband detection window

off-line to on-line signals is plotted in Fig. 7. This ratio is very small for the LIF measurements owing to the essentially negligible common background, whereas the ratio is much larger for PLIF measurements and demonstrates the expected result, i.e., as the level of doping rises, the ratio decreases owing to the increase in NO signal relative to the background.

To convert PLIF images to quantitative NO concentration measurements, Cooper et al. [6] and Ravikrishna et al. [7] utilized a single-point scaling technique to collapse the PLIF profiles to within the accuracy bars of more quantitative laser-saturated fluorescence (LSF) measurements. Cooper et al. [6] were able to quantify time-average PLIF data since the electronic quenching rate coefficient was found to be essentially uniform in the central region of the LDI spray flame. Recognizing that the background is pressure dependent [13], a complete spectral study would be required to identify an on-line/off-line scheme with a common background in the 68-nm detection window of the ICCD camera. As such an exhaustive study is not the focus of this paper, we will simply utilize a single-point scaling of the measurements to quantify the PLIF data.

3.3 PLIF experimental method

The procedure to convert a PLIF image to an NO concentration field is very similar to that for LIF. We utilized an on-line wavelength (225.58 nm) resonant with the $Q_2(26.5)$ transition of NO. NO was doped into the flame so as to achieve doped flow-field concentrations of 86, 65, 44, 22, and 0 ppm. For each doping condition, an image was recorded corresponding to the on-chip summation of 1200 laser shots. The laser was then tuned to an off-line wavelength (225.53 nm) and a similar image was recorded. The data were then processed as follows: (i) the flame luminosity was subtracted from the initial on- and off-line images by employing a similar image with no laser beam passing through the probe volume; (ii) these on- and off-line images were normalized by the distribution of energy in the laser sheet via a 20-shot image which recorded Rayleigh scattering in air; and (iii) the normalized off-line image was subtracted from the normalized on-line image. To directly compare the PLIF data with those obtained by LSF and LIF, 1-mm squares were averaged throughout the image and horizontal stripes were extracted corresponding to $h = 5$, 10, and 20 mm. The slightly larger sampling volume of the PLIF measurements compared to that of the LIF measurements was chosen to increase the signal-to-noise ratio. A $1\,\text{mm} \times 1\,\text{mm}$ region along the centerline at each height was utilized to obtain a calibration slope from the five doping levels. In a manner identical to the LIF measurements, the radial profiles at each axial height (5, 10, and 20 mm) were then corrected with a fluorescence calibration specific to that height. To better compare the extracted PLIF data with the LIF data, the data sets for both measurements are not corrected for skewing with the mirror/average procedure.

3.4 NO PLIF profiles

The PLIF measurements demonstrated qualitatively similar profiles, but were a nominal 16% smaller than the quantitative LIF measurements. This depression results from the increased background for the PLIF detection scheme, as discussed previously. Though a 16% discrepancy is not excessively large, more accurate data can be achieved by scaling the PLIF measurements using a ratio of the LIF/PLIF data at the centerline 10-mm axial height. The scale factor is ≈ 1.19. The result of such a scaling is pictured in Fig. 8, with the PLIF data now collapsed to within the accuracy bars of the LIF data.

Several precautions must be noted in regard to the quantification of PLIF data. Since the background for the two excitation wavelengths is large and not common in the PLIF detection window, the off-line/on-line fluorescence signal depends on the doping level. Moreover, since we are using a subtraction procedure, the variation in this ratio throughout the flame would normally cause erroneous results and the PLIF data would not scale correctly with the LIF data. In addition, if the background itself shifts owing to changes in the concentrations of interfering species such as O_2 or owing to temperature gradients, then an effective collapse such as that demonstrated in this paper would be difficult to achieve. However, Fig. 4 demonstrates a very uniform NO concentration in the central region of the LDI spray flame. This uniformity in a minor species such as NO likely implies uniformity

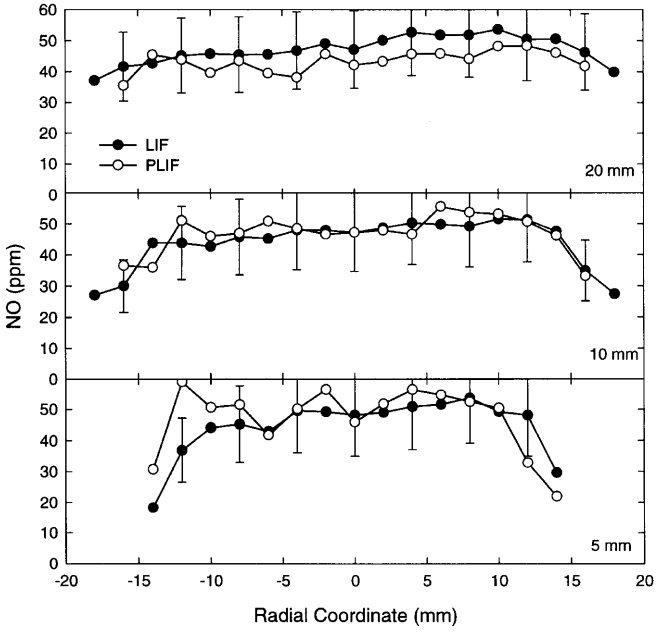

Fig. 8. Comparison of the corrected PLIF measurements to the LIF measurements. The PLIF measurements fall within the accuracy bars of the LIF data, emphasizing the utility of the PLIF technique for LDI spray flames when a scaling point can be obtained from quantitative LIF data

in the major species. The temperature variation within the 5-mm to 20-mm region along the central axis has been shown to be $\approx 10\%$ [15]. This uniformity in species concentrations and temperature leads to a constant off-line/on-line ratio that allows effective calibration. Hence, the LDI flame, with its recirculation zone, is uniquely suited to quantitative PLIF images, which thus permits this diagnostic tool to be used for the detection of NO.

4 Conclusions

Quantitative LIF measurements of NO concentration have been obtained in a LDI flame fueled with liquid heptane at 4.27 atm so as to assess the utility of PLIF as a diagnostic technique for high-pressure spray flames. The LIF profiles reveal a uniform distribution of NO (ppm) throughout the flame. Spectral studies for a PLIF detection scheme confirm that a broad detection window of 68 nm is plagued by fluorescence interferences from rogue species. Nevertheless, PLIF profiles can be quantified through a single-point scaling with the more quantitative LIF data owing to the unique attributes of the LDI flame.

The end-goal of this work is to develop a laser-induced fluorescence technique capable of measuring quantitative NO concentrations in 1–10 atm LDI-based spray flames. Considering the excellent profile comparisons between the two LIF-based techniques presented in this paper, we conclude that qualitative PLIF measurements of [NO] at high pressure can be scaled in a similar fashion by using a single calibrated point so as to produce quantitative PLIF measurements of NO.

Acknowledgements. This research was funded by the National Aeronautics and Space Administration (Lewis Research Center) through General Electric Aircraft Engines, Cincinnati, OH. C.S. Cooper acknowledges support by a National Defense Science and Engineering Graduate Fellowship during this research and current support by an ASME Graduate Teaching Fellowship. We thank our project technical monitors, Mr. Chi Lee of NASA and Mr. Paul Sabla of General Electric. Bob Willis of Purdue Mechanical Engineering machined the burner and the helical swirlers.

References

1. M.G. Allen, K.R. McManus, D.M. Sonnenfroh: AIAA Paper No. 94-2913, presented at the 30th Joint Propulsion Conference, June 1994 (American Institute of Aeronautics and Astronautics, New York 1994)
2. M.G. Allen, K.R. McManus, D.M. Sonnenfroh, P.H. Paul: Appl. Opt. **34**, 6287 (1995)
3. B.L. Upschulte, M.G. Allen, K.R. McManus: *Twenty-Sixth Symposium (International) on Combustion* (The Combustion Institute, Pittsburgh, PA 1996), pp. 2779–2786
4. R.J. Locke, Y.R. Hicks, R.C. Anderson, K.A. Ockunzzi, G.L. North: AIAA Paper No. 95-0173, presented at the 33rd Aerospace Sciences Meeting & Exhibit, January 1995 (American Institute of Aeronautics and Astronautics, New York 1995)
5. C.S. Cooper, N.M. Laurendeau: Combust. Sci. Technol. **127**, 363 (1997)
6. C.S. Cooper, R.V. Ravikrishna, N.M. Laurendeau: Appl. Opt. **37**, 4823 (1998)
7. R.V. Ravikrishna, W.P. Partridge, Jr., and N.M. Laurendeau: Combust. Sci. Technol. **144**, 79 (1999)
8. J.R. Reisel, C.D. Carter, N.M. Laurendeau: Combust. Sci. Technol. **91**, 271 (1993)
9. C.S. Cooper, N.M. Laurendeau: Appl. Opt. **36**, 5262 (1997)
10. J.M. Harris, F.E. Lytle, T.C. McCain: Anal. Chem. **48**, 2095 (1976)
11. C.S. Cooper, N.M. Laurendeau: accepted for publication to Meas. Sci. Technol. (1999)
12. W.P. Partridge, M.S. Klassen, Jr., D.D. Thomsen, N.M. Laurendeau: Appl. Opt. **34**, 4890 (1996)
13. D.D. Thomsen, F.F. Kuligowski, N.M. Laurendeau: Appl. Opt. **36**, 3244 (1997)
14. C.S. Cooper, N.M. Laurendeau: submitted for publication to Combust. Sci. Technol. (1999)
15. C.S. Cooper, N.M. Laurendeau: submitted for publication to Combust. Flame (1999)
16. K. Lee, B. Chehroudi: J. Propul. Power **11**, 1110 (1995)
17. R.J. Kee, J.F. Grcar, M.D. Smooke, J.A. Miller: Sandia Report SAND85-8240 (1985)
18. H.S. Alkabie, G.E. Andrews: ASME Paper No. 89-GT-322, presented at the International Gas Turbine and Aeroengine Congress and Exposition, June 1989 (American Society of Mechanical Engineers, New York 1989)
19. T. Terasaki, S. Hayashi: *Twenty-Sixth Symposium (International) on Combustion* (The Combustion Institute, Pittsburgh, PA 1996), pp. 2733–2739